Composites: Part A 179 (2024) 107992

Contents lists available at ScienceDirect

Composites Part A

journal homepage: www.elsevier.com/locate/compositesa

# Ballistic performance of bio-inspired hybrid interleaved composite structures suitable for aerospace applications

M.Erfan Kazemi [a,*], Victor Medeau [a], Yanhong Chen [b], Ziwen Xu [b], Nik Petrinic [b], Emile Greenhalgh [a], Paul Robinson [a], James Finlayson [c], Silvestre T. Pinho [a]

[a] Department of Aeronautics, Imperial College London, Exhibition Rd, South Kensington, London SW7 2AZ, UK
[b] Department of Engineering Science, University of Oxford, Parks Road, Oxford OX1 3PJ, UK
[c] Composites - Structural Systems Design, Rolls-Royce, PO Box 31, Derby DE24 8BJ, UK

ARTICLE INFO

*Keywords:*
Aircraft engine casing demonstrator
Bio-inspired hybrid interleaved layup
Carbon-fibre-reinforced polymer (CFRP)
High-velocity impact (HVI)

ABSTRACT

We investigate the ballistic performance of an aircraft engine containment casing demonstrator, made of composite materials with a novel bio-inspired hybrid interleaved design, under high-velocity impact (HVI) at a specific angle. Firstly, we apply a bio-inspired (BI) helicoidal design to develop a large-scale monolithic laminate concept made of carbon fibre-reinforced polymer (CFRP). Then, we hybridise the developed BI laminate concept with interleaved blocks of Zylon fibre (PBO)-reinforced polymer to develop a large-scale BI hybrid interleaved laminate concept. We then further hybridise the developed BI hybrid concept with titanium (Ti) foils (located at the impact face) so that in total we have three large-scale laminate concepts. We manufacture 6 large-scale laminates from each concept with dimensions of 225 × 225 mm and a target areal weight of 0.95 g/cm$^2$. We then test them (perpendicularly) under HVI ranging from 150 to 300 m/s to obtain the ballistic limit and energy dissipation. Secondly, after selecting the best-performing developed laminate concept, we scale it up to develop industrial demonstrator panels with a target areal weight of 1.5 g/cm$^2$ and dimensions of 550 × 360 mm. We test the panels under HVI at an angle of 55° with a larger and heavier projectile, to more closely represent a fan blade-off event onto the engine casing. The results of the large-scale laminate concept tests show that the BI hybrid interleaved CFRP/PBO concept outperformed the rest of the concepts with 54% and 34% improvement in energy dissipation compared to that of quasi-isotropic (QI) and the BI monolithic CFRP, respectively. Our results show that small-scale designs for HVI-resistant CFRP-based laminates cannot be simply assumed to exhibit an equivalent performance for industrial applications with thicker laminates, heavier projectiles and impacts at an angle.

## 1. Introduction

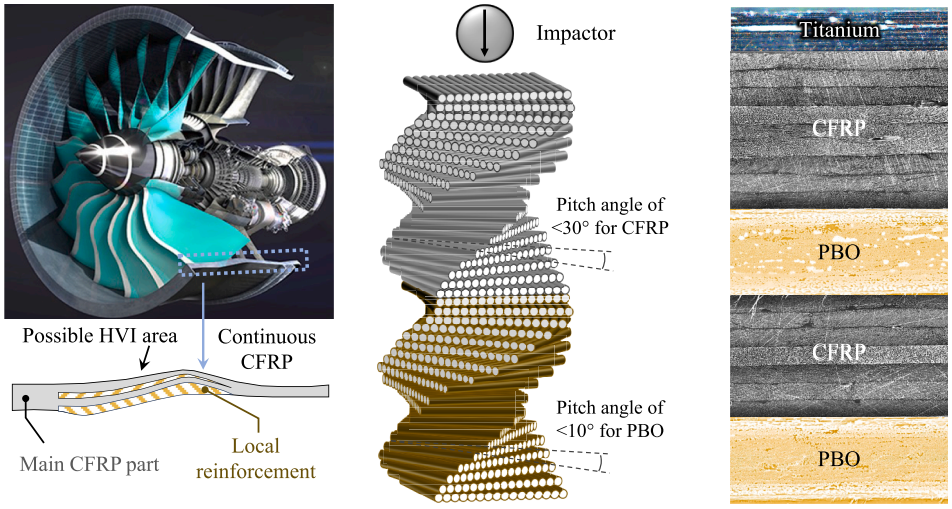
During flight, bird strikes on the nose of the aircraft, the leading edge of the wing(s), the inlet of an engine during take-off/landing [1–5], or engine blade-off events onto the containment casing [6–9], are a cause for concern. These incidents represent high-velocity impact (HVI) events and can damage the aircraft and thus compromise the safety of the people onboard.

As composite structures are being increasingly used in the aerospace industry [10–12], innovative lightweight damage-tolerant composites solutions should be developed tailored for areas that are susceptible to HVI [13–15]. Among composite structures, carbon fibre-reinforced polymers (CFRP) provide excellent solutions due to their high specific in-plane mechanical properties [16]. However, they are brittle, which makes them vulnerable to out-of-plane loadings such as HVI [17,18]. Improving the response of CFRP to HVI events has therefore become an active area of research.

In this regard, hybridising CFRP with high-strain materials, such as metal alloys, high strain-to-failure fibre reinforcements, and foams (among others) has been reported as a successful approach to improve the response [13,19–24]. Hybridising can be applied by implementing blocks of hybridising materials at either side of composite laminates (called bulk hybrid) or distributing blocks of hybridising materials through the thickness of composite laminates (called interleaved hybrid) [25–27]. However, hybridisation usually reduces the in-plane mechanical properties of CFRP, which might affect the performance of

* Corresponding author.
*E-mail address:* m.kazemi@imperial.ac.uk (M.Erfan Kazemi).

https://doi.org/10.1016/j.compositesa.2023.107992
Received 12 September 2023; Received in revised form 19 December 2023; Accepted 27 December 2023
Available online 28 December 2023
1359-835X/© 2024 The Authors. Published by Elsevier Ltd. This is an open access article under the CC BY license (http://creativecommons.org/licenses/by/4.0/).

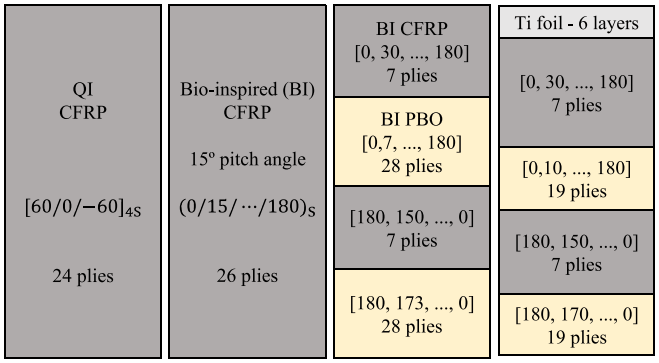



(a) A cut of an aircraft engine (courtesy of Rolls-Royce plc) (b) Bio-inspired (BI) design (c) Interleaved hybrid design

**Fig. 1.** (a) A cut of an aircraft engine showing its containment casing cross-section and the corresponding schematic at the bottom, (b) bio-inspired helicoidal layup and (c) hybrid interleaved designs.

composite structures in critical in-plane loadings. As a result, depending on the application, relevant design criteria such as maintaining suitable in-plane mechanical properties should be considered when developing hybrid CFRP-based composite structures. In this regard, Kazemi et al. [28] developed a range of hybrid CFRP composite structures, while maintaining the ratio of CFRP as 80% of (the mass of) the whole structure and keeping the areal weights constant. They found that among various applied hybridising materials (such as glass, Zylon and Dyneema fibres, as well as ceramic, foam, titanium and shape memory alloy sheets), Zylon fibre (PBO)-reinforced polymers performed best in a hybrid CFRP composite laminate under HVI.

Another approach to enhance the damage tolerance of composite structures in out-of-plane loadings is to apply bio-inspired (BI) layups. In recent years, researchers have explored unconventional lamination sequences inspired by naturally occurring impact-resistant microstructures, such as Bouligand structures [29], to enhance the resistance of composite structures. These Bouligand-like structures can be found in various animals, including the mantis shrimp [30]. The microstructure of the mantis shrimp's dactyl club includes a periodic region containing multiple repetitions of the Bouligand unit, arranged along the thickness direction. Each Bouligand unit features a helicoidal layup characterised by very small inter-ply (pitch) angles, resulting in a total rotation of 180°




(a) QI CFRP (baseline) (b) BI CFRP (c) BI CFRP/PBO (d) BI Ti/CFRP/PBO

**Fig. 2.** Schematics of the layups of the developed large-scale laminate concepts.

within each unit. Concerning this, most of the studies in the literature have been dedicated to the response of composite structures with BI helicoidal layups for low-velocity impact (LVI) applications. Ginzburg et al. [31] and Mencattelli and Pinho [30] investigated the damage tolerance of BI helicoidal composites under LVI. They concluded that the BI helicoidal layups, compared to traditional quasi-isotropic (QI) layups, are more effective at dissipating energy through extended delamination and the migration of helicoidal matrix cracks from one ply to nearby plies. Further researchers also observed that the response of BI composite structures under LVI [32–35] was superior to a baseline.

However, concerning the HVI response of BI composite structures, the findings from the literature are limited and sometimes counter-intuitive. Liu et al. [30] studied the response of three BI monolithic laminates, made of CFRP, Kevlar and polyethylene fibre-reinforced polymers subject to HVI. They reported that the helicoidal CFRP laminate with small inter-ply (pitch) angles outperformed its cross-ply and QI counterparts, while the other two helicoidal laminates performed poorly, relatively to the corresponding cross-ply laminates, as the Kevlar and polyethylene fibres were reported tougher. Wang et al. [36] also found that BI aramid-based laminates performed worse than QI and cross-ply counterparts. Nonetheless, Abir et al. [37] experimentally and theoretically investigated the ballistic performance of BI CFRP composites and found that the ballistic limit of the BI helicoidal layup was about 8% and 15% higher than their equivalent cross-ply and QI counterparts, respectively.

In the aforementioned studies (and in general in the literature), industrial design constraints are often neglected. In this study, we focus on critical aerospace applications such as an engine containment casing (Fig. 1 (a)), and we, therefore, constrained our designs to retain suitable in-plane properties (by keeping at least 50% CFRP), to aim for constant areal weight, and to not significantly increase the thickness.

In this paper, firstly, we apply a novel design methodology consisting of BI and hybrid interleaved designs to develop various large-scale laminate concepts (225 × 225 mm and ~ 6.5 mm thick). We then test the developed large-scale laminate concepts, perpendicularly, under HVI to obtain their ballistic performance and failure modes. Then, based on the obtained results, we select the best-performing laminate concept and scale it up to develop and manufacture industrial demonstrator panels (550 × 360 mm and ~ 10.5 mm thick). For these, we change the test setup configuration and impact the developed industrial demonstrator panels at an angle of incidence of 55° (based on the

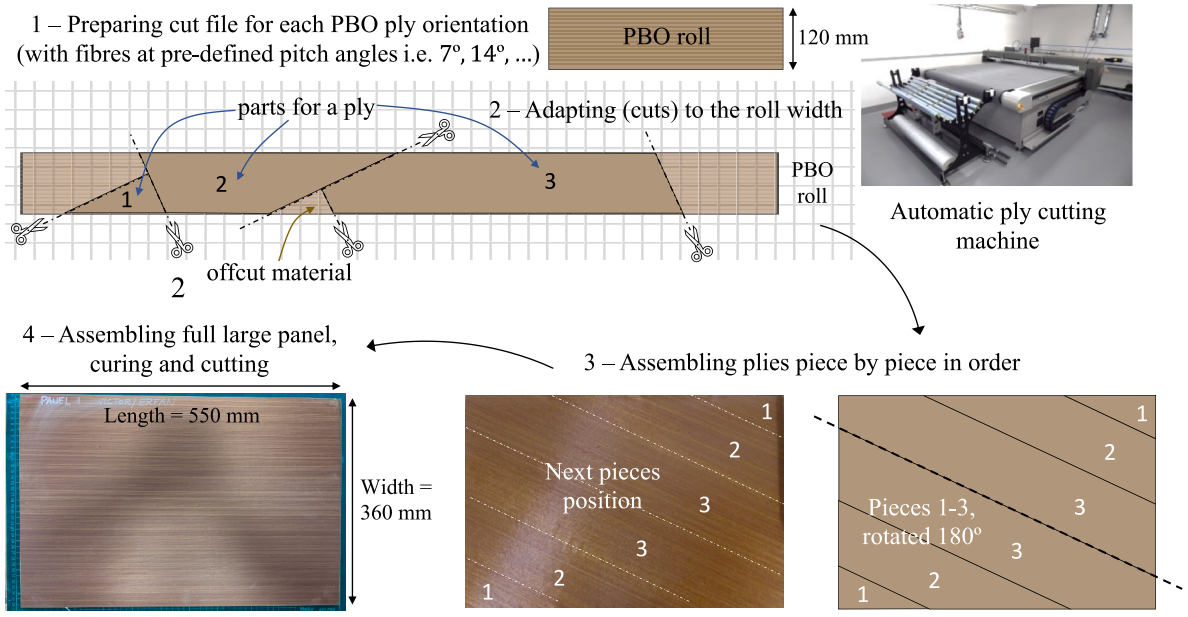



**Fig. 3.** Overview of the required fabricating process for manufacturing large laminates from 120 mm wide PBO and 75 mm wide CFRP prepreg rolls.

recommendation from our industrial partner) with a larger and heavier projectile to more closely represent a fan blade-off event onto the casing. Finally, we investigate the performance of impacted demonstrator panels and compare their response with that of the large-scale laminate concepts impacted perpendicularly under HVI.

## 2. Large-scale laminates

### 2.1. Methodology and materials

To develop large-scale laminate concepts, we applied a novel design methodology consisting of BI and hybrid interleaved designs. Concerning the BI design, we used a helicoidal layup, see Fig. 1 (b). Based on the thickness of CFRP (and to have a full rotation of plies), we used pitch angles of less than 30° to develop a BI monolithic CFRP laminate concept, Fig. 2. To hybridise the monolithic CFRP laminate concept, we implemented BI interleaved blocks of Zylon fibre (PBO)-reinforced polymers through the thickness with pitch angles of less than 10° to develop one of the hybrid laminate concepts, and with addition to titanium (Ti) foils to develop another laminate concept, Fig. 1 (b) and (c). The reason for selecting different pitch angles in CFRP and PBO blocks is due to the difference between the areal weight (or the thickness) of the CFRP and PBO prepregs, Fig. 2. As CFRP prepregs are thicker, and we need to have a full rotation of plies in a layup with specific areal weight and hybridising ratio, the number of thick-ply CFRP plies would be lower (compared to the number of ultra-thin PBO plies). This allows us to select smaller pitch angles and thus more plies in a fixed areal weight for a PBO block. Kazemi et al. [38] showed that inserting blocks of hybridising materials through the thickness of composite laminates better improves the HVI response compared to placing all the hybridising material as one block at the back face. As mentioned, to ensure suitable mechanical properties, we kept the ratio of the mass of the hybridising material(s) to the mass of the whole laminate concept less than 50%.

Regarding materials, we used a uni-directional (UD) aerospace-grade CFRP epoxy system (confidential, information withheld by the sponsor) with an areal weight of 280 gsm and a thickness of 0.25 mm to develop the BI monolithic laminate concept and also to develop a quasi-isotropic (QI) monolithic baseline for comparison. To hybridise the CFRP laminate concept, we used ultra-thin UD Zylon (PBO) fibre-reinforced polymers containing Zylon-HM545T fibres (with the tenacity of 5.8 GPa, modulus of 270 GPa and elongation at break of 2%) and ThinPreg™ 513 (TP513) toughened epoxy system (with 3.1 GPa tensile modulus and 54 MPa tensile strength). Ultra-thin ply Zylon-HM545T/TP513 (PBO) prepreg has an areal weight of 25 gsm and a thickness of 0.021 mm. Titanium foils (ASTM B265 Grade 2) with a thickness of 0.5 mm, attached with 3 M epoxy resin films (together without any surface treatment) also have been used for one of the hybrid laminate concepts.

### 2.2. Manufacturing and testing

To manufacture the large-scale laminate concepts (and also demonstrator panels in the next section), based on the width of the rolls of PBO (120 mm) and CFRP (75 mm) and the required pitch angle (provided in Fig. 2), we first generated cut files in CAD for the rolls to cut them on an automatic ply cutting machine, step 1, see Fig. 3. We then laid down the roll of the materials on the automatic ply cutting machine and adapted cuts to the width of the roll, step 2. Then, we cut all the plies needed for the full width of the laminate concepts and continued this for all the plies with different pitch angles for both PBO and CFRP plies and

**Table 1**
Layups and properties of the developed large-scale laminate concepts.

| Laminate name | Layup (with their pitch angle) | Number of specimens | Thickness (mm) | Hybridising material(s) ratio | Areal weight ($g/cm^2$) |
|---|---|---|---|---|---|
| QI* CFRP (Baseline) | $(60/0/\text{-}60)_{4S}$ | 2 | 6.4 | 0 | 0.94 |
| BI** CFRP | $(0/15/\ldots/180)_S$ | 6 | 7.1 | 0 | 1.12 |
| BI CFRP/PBO | (0/30/…/180), (0/7/…/180), (180/150/…/0), (180/173/…/0) | 6 | 6.8 | 0.43 | 1.02 |
| BI Ti/CFRP/ PBO | $Ti_6$, (0/30/…/180), (0/10/…/180), (180/150/…/0), (180/170/…/0) | 6 | 6.5 | 0.43 | 1.05 |

* QI: quasi-isotropic.
** BI: bio-inspired.

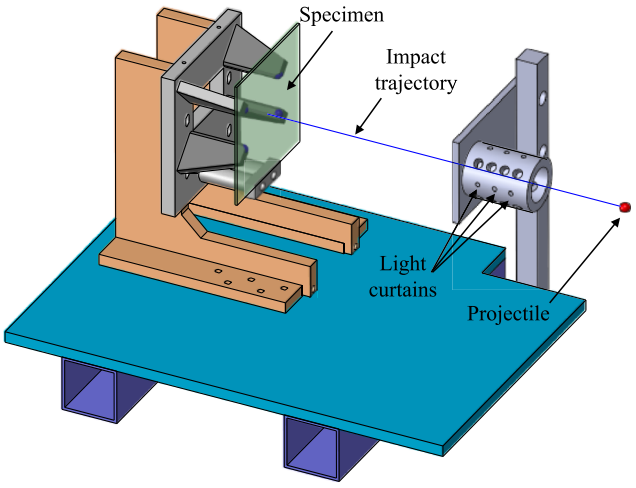



**Fig. 4.** Schematic of the test setup for the large-scale laminate concepts.

placed the cut pieces beside each other, step 3. Finally, in step 4, we assembled the blocks to have the full laminates, cured and cut them based on the dimensions of the large-scale laminates, 225 × 225 mm (or demonstrator panels, 550 × 360 mm provided in the next section). We co-cured PBO plies and titanium foils with CFRPs (information regarding the curing of CFRP cannot be disclosed due to its commercially sensitive nature). We manufactured 6 laminates for each of the concepts and also manufactured QI baseline laminates for comparison. It is worth mentioning that hybridising materials (such as PBO fibres) change the weight of the laminate, its stiffness and strength (compared to a CFRP laminate with the same thickness). As a result, there is value in addition to making comparisons with equivalent areal weight. Thus, we aimed to manufacture all the large-scale laminate concepts with a target areal weight of 0.95 g/cm$^2$. We provide information regarding the layups and properties of the manufactured large-scale laminate concepts in Table 1.

To test the developed large-scale laminate concepts under HVI, we used a single-stage gas gun firing spherical steel balls with a diameter of 16 mm (embedded in foam sabots) to impact the laminates from 150 to 300 m/s, perpendicularly, Fig. 4. We used two elastic (rubber) bands to hold specimens vertically against a simply-supported boundary conditions test rig, which have 4 bearing balls on its corners (with diameters of 20 mm). The size of the support window formed by the bearing balls is 125 × 75 mm. In front of each specimen, we mounted three light curtains onto a hollow cylindrical component that was axially aligned with the trajectory of the projectile, and we connected the light curtains to an oscilloscope to measure the (initial) impact velocity. We also connected the first light curtain (the rightmost in Fig. 4) to a signal splitter to trigger the flashlight as well as two high-speed cameras (Photron SA5) that we installed on the top and the side of the test setup. Before testing, we placed a steel ruler in the trajectory of the projectile and took two photos of the ruler using the two cameras to obtain calibration scales (i.e., the physical length of a pixel), which we used to determine the velocity history of the projectile from the recorded videos. We recorded (high-speed) images at a frame rate of 40,000 fps to track the journey of the projectile and calculate rebound/perforation velocity.

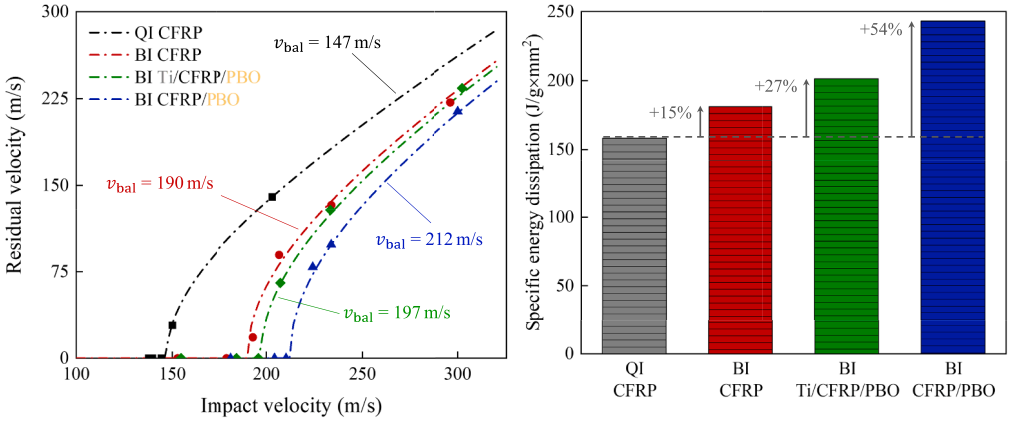
### 2.3. Results and discussion: Large-scale laminates

Fig. 5 (a) and (b) show the HVI test results of the developed large-scale laminate concepts including: QI CFRP baseline, BI monolithic CFRP, BI hybrid interleaved CFRP/PBO, and BI hybrid interleaved Ti/CFRP/PBO impacted from 150 to 300 m/s. To obtain the ballistic limit we plotted the impact velocity against residual velocity for laminates that got perforated (Fig. 5 (a)). We used the Lambert-Jonas equation [39] to fit the experimental data:

$$v_{res} = A\left(v_{ini}^2 - v_{bal}^2\right)^{1/2} \quad (1)$$

where $v_{res}$ is the residual velocity, $v_{ini}$ is the impact velocity and $v_{bal}$ is the ballistic limit. As Fig. 5 (a) shows, changing the layup from QI to BI in the monolithic CFRP increased the ballistic limit from 147 to 190 m/s, showing about a 30% improvement. By hybridising the BI CFRP monolithic laminate with interleaved blocks of PBO fibres, the ballistic limit increased further and reached about 210 m/s, showing about a 43% improvement compared to that of the QI baseline. However, by removing some of the PBO fibres (located at the back face) and replacing them with titanium (Ti) foils (at the impact face), the ballistic limit decreased to around 197 m/s (yet still 34% higher than that of the QI CFRP baseline). The reduction in the ballistic limit is due to both changing the type and the position of the hybridising material (here Ti foils vs PBO fibres, and impact vs back face). We should emphasise that we kept the ratio of the mass of hybridising material(s) to the whole mass of the CFRP-based laminate concepts at less than 50% as a design constraint to ensure suitable in-plane mechanical properties.

To compare the energy dissipation of the impacted laminates meaningfully, we used specific energy dissipation, which is the ratio of the absorbed energy (impact energy minus residual energy) divided by the areal weight of each specific laminate. Fig. 5 (b) exhibits the specific energy dissipation of the large-scale laminate concepts that got penetrated/perforated, which shows a similar trend to what we observed for




(a) Impact vs. residual velocity (b) Specific energy dissipation

**Fig. 5.** The ballistic response of the large-scale laminate concepts under HVI.

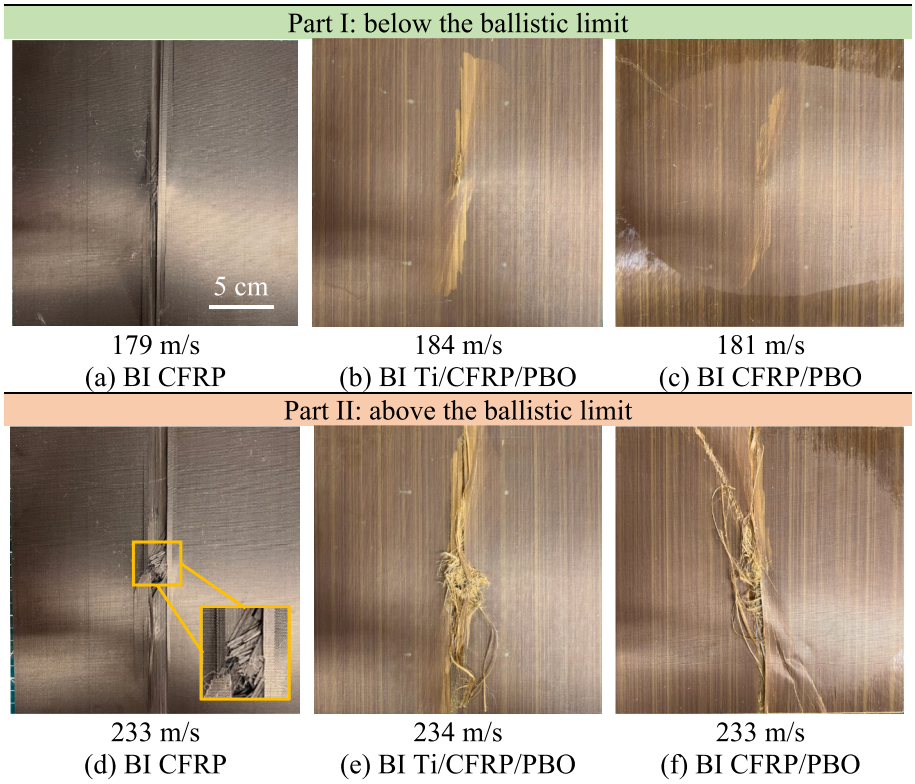



**Fig. 6.** Back face images of the large-scale laminate concepts impacted below and above their ballistic limits.

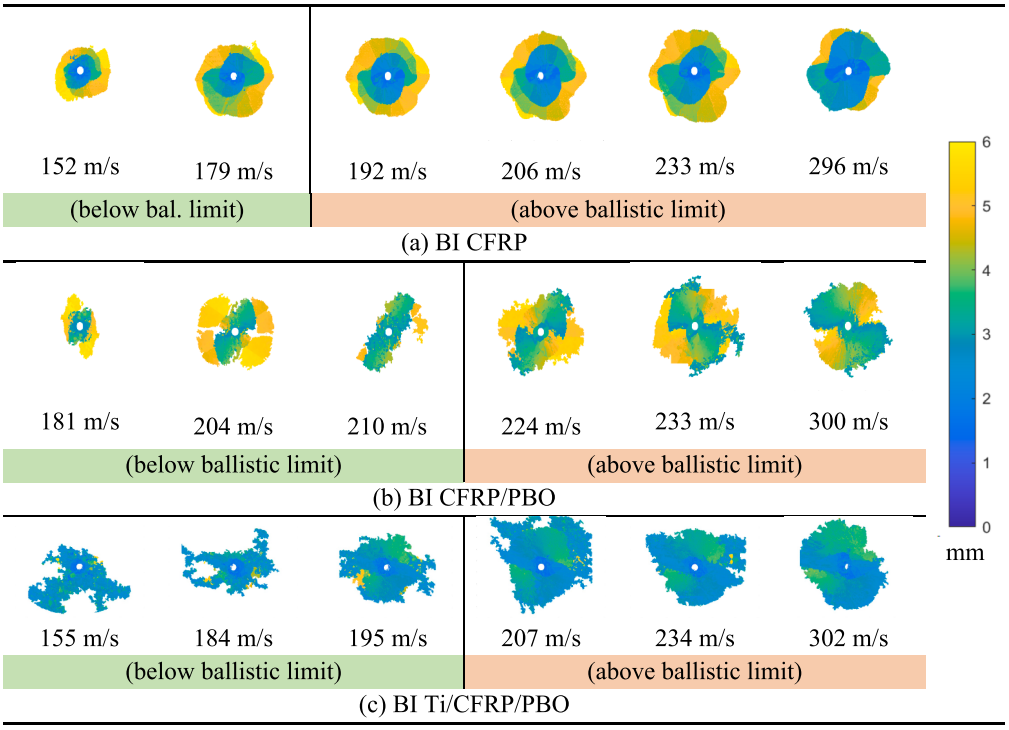



**Fig. 7.** C-scan images consisting of delamination (areas) of the large-scale BI CFRP, BI CFRP/PBO and BI Ti/CFRP/PBO laminate concepts impacted from 150 to 300 m/s (the vertical bar on the right shows C-scan depth).

the ballistic response. Fig. 5 (b) shows that the specific energy dissipation of the QI monolithic CFRP increased by about 15% when the layup changed from QI to BI, and by 54% when we replaced the layup of the QI monolithic CFRP with the BI hybrid interleaved CFRP/PBO.

Fig. 6–9 illustrate images of post-mortem analysis of selected impacted large-scale laminate concepts. Fig. 6 presents the back face images of the BI CFRP, BI Ti/CFRP/PBO and BI CFRP/PBO impacted at 180 m/s (below their ballistic limits) and 230 m/s (above their ballistic

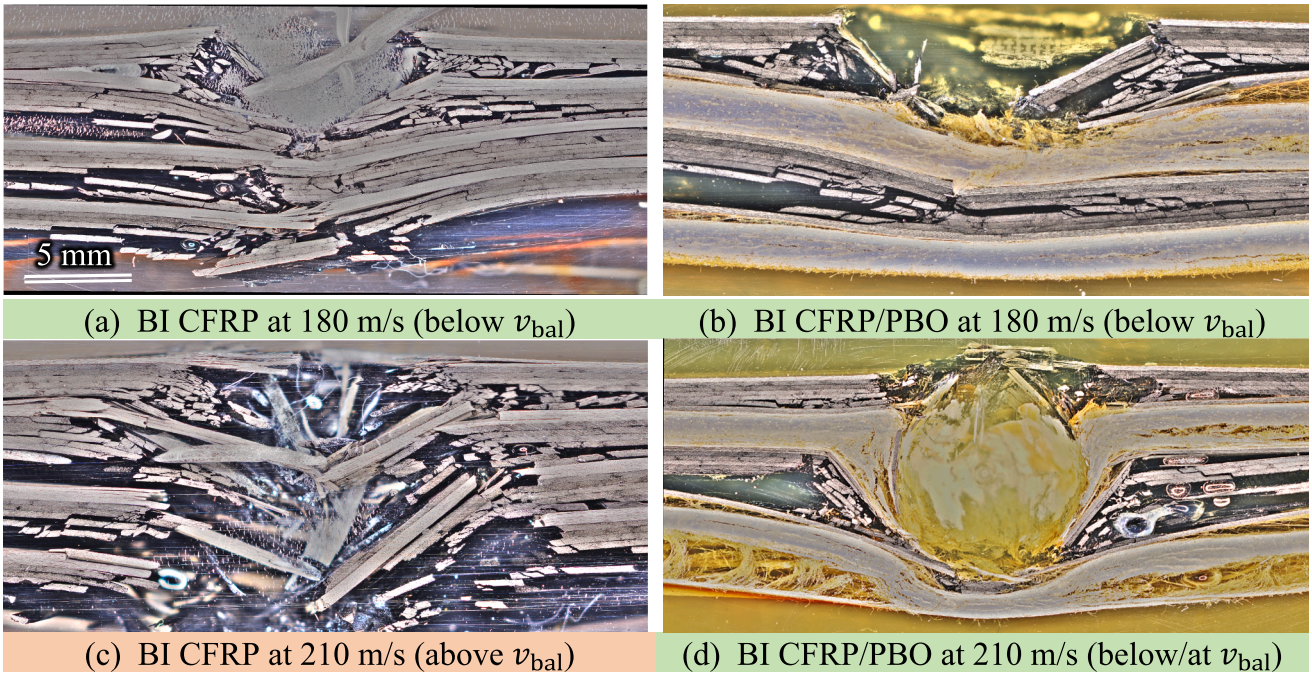



**Fig. 8.** Cross-sections of the BI CFRP and the BI hybrid interleaved CFRP/PBO impacted at 180 and 210 m/s.

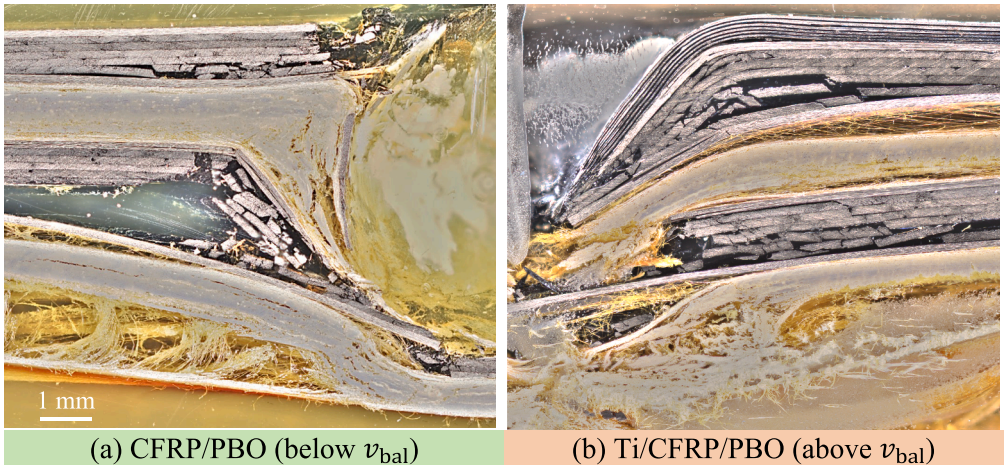



**Fig. 9.** Cross-sections of large-scale CFRP/PBO and Ti/CFRP/PBO laminate concepts impacted at 210 m/s.

limits). At 180 m/s, the BI monolithic CFRP underwent multiple fibres fracture at the back face, Fig. 6 (a), while the BI Ti/CFRP/PBO suffered from very minor PBO fibre failure, Fig. 6 (b). However, in the BI CFRP/PBO, Fig. 6 (c), we did not observe any fibre damage/failure at the back face compared to that of the BI CFRO or BI Ti/CFRP/PBO, suggesting other than the deflection of PBOs, extra energy dissipating mechanisms should have happened inside the laminate.

By increasing the impact velocity to 233 m/s (above the ballistic limit), we observed fibres spalling and more damage at the back face of the BI CFRP laminate, Fig. 6 (d). We also detected failed CFRP fibres in a helicoidal way around the impact zone (Fig. 6 (d)). Regarding both of the hybrid interleaved laminates impacted at 233 m/s, we observed significant damage and failure of PBO fibres as well as delamination at the back face in helicoidal manners, Fig. 6 (e,f).

Fig. 7 shows the C-scan images consisting of delamination (areas) of the large-scale BI CFRP (Fig. 7 (a)), BI CFRP/PBO (Fig. 7 (b)) and BI Ti/CFRP/PBO (Fig. 7 (c)) laminate concepts impacted from 150 to 300 m/s. For performing C-scan analysis, we used a Technitest Ultrasonic NDT C-scan machine using a scan speed of 100 mm/s with an interval of 0.2 mm. For all laminates, when the impact velocity increased from 150 m/s and reached the respective ballistic limit for each laminate, the extent of matrix cracks and delamination increased. In all impacted laminate concepts, the C-Scan images depict the initiation of the helicoidal matrix cracks and helicoidal delamination from the impact face (in dark blue), which propagated in size towards the back face (in yellow/orange; the reason for the limited delamination area in the BI CFRP/PBO laminate impacted at 210 m/s (Fig. 7 (b)) is due to extra deformation in the PBO block caused by the sandwiched projectile (compared to the rest of the laminates). Thus, the set configuration (of 6 mm) for measuring the delamination depth was unable to capture the total area of delamination). We should emphasise that the presence of the Ti foils in the BI TI/CFRP/PBO laminate concept created noise during the C-scan, which makes the observation of matrix cracks and delamination difficult, Fig. 7 (c).

Fig. 8 and Fig. 9 present the cross-sections of selected large-scale laminate concepts impacted at 180 m/s and 210 m/s. Fig. 8 (a) shows

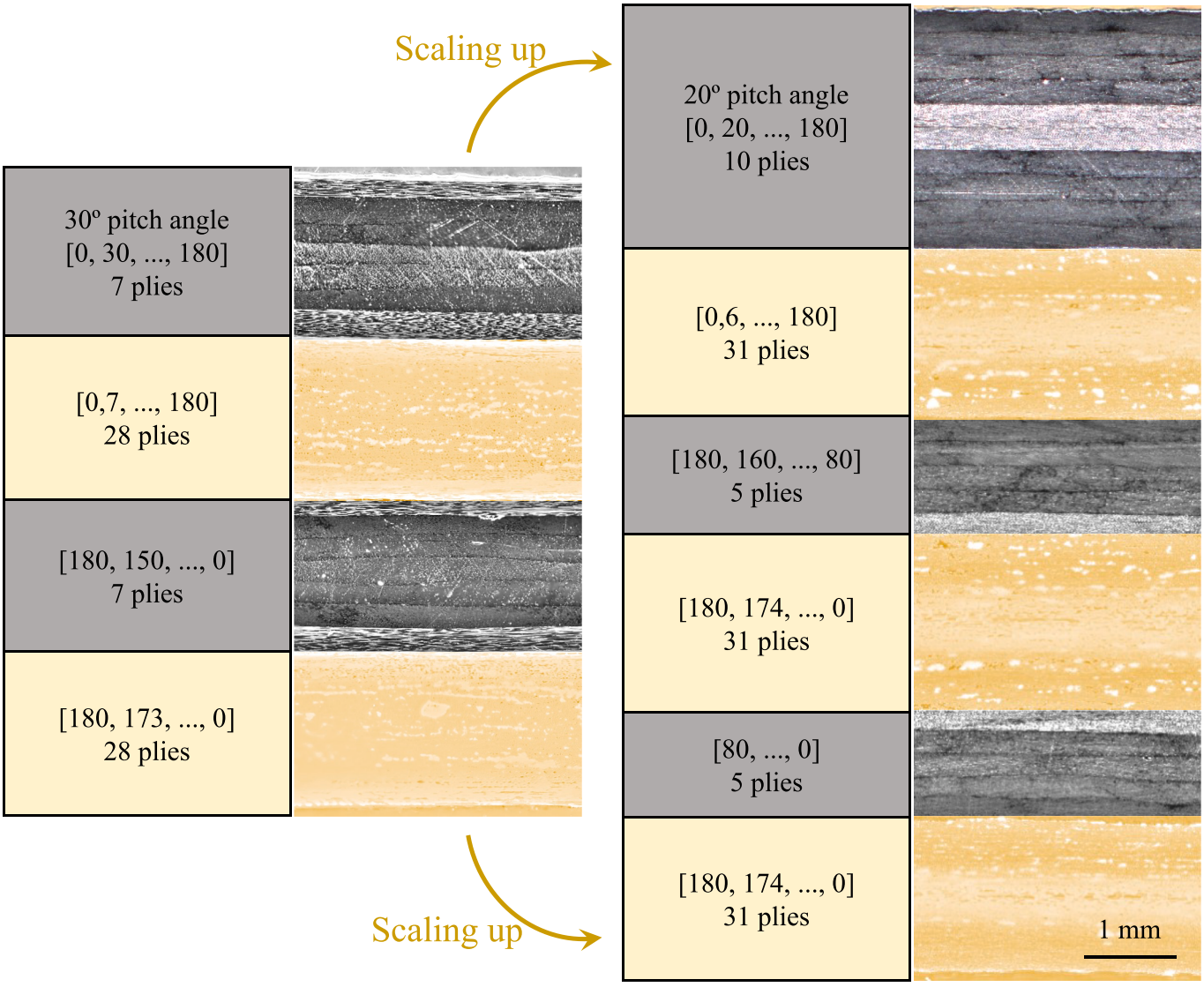



**Fig. 10.** The design and cross-section of the CFRP/PBO industrial demonstrator panel (scaled) compared to the large-scale laminate concept.

that at 180 m/s, the BI monolithic CFRP laminate underwent some delamination and fibre failure around the impact zone. For this laminate, we can observe that the failure mechanisms are crushing and fragmentation at the impact face, shear plugging and (limited) tensile failure. Although shear plugging and tensile failure are the dominant failure mechanisms for the BI CFRP laminate, as reported in the literature [40], shear plugging dissipates limited energy during HVI.

By replacing the BI monolithic layup with the BI hybrid interleaved one, we did not observe any fibre failure at the back face in the BI CFRP/PBO, Fig. 8 (b). The presence of the middle PBO block precluded shear plugging and resisted penetration. Moreover, the high failure strain of PBO fibres let the laminate deform significantly with extensive matrix cracks and delamination that happened inside the blocks of PBO. Nonetheless, the CFRP blocks suffered from fibre fracture, delamination and matrix cracks (Fig. 8 (b)).

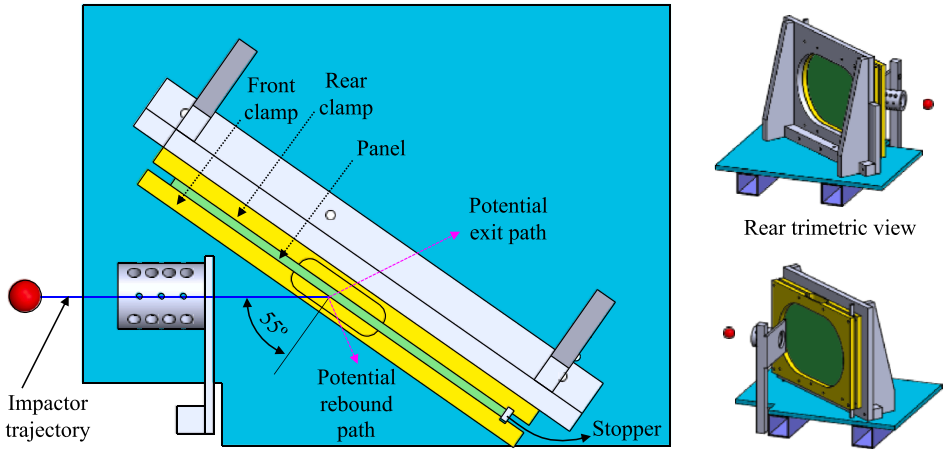
By increasing the velocity from 180 to 210 m/s, the BI CFRP perforated, Fig. 8 (c). Fig. 8 (c) shows that the laminate underwent significant shear plugging and damage is very localised and limited around the projectile. However, the BI CFRP/PBO did not perforate and the projectile got sandwiched inside the laminate (penetration occurred), Fig. 8 (d) and Fig. 9 (a). By analysing the cross-section of the BI CFRP/PBO impacted at 210 m/s, we detect extensive delamination in the last block of the PBO (Fig. 8 (d)). The presence of multiple interfaces between the blocks of CFRP and PBO creates more potential delamination zones, which contributed further to the higher energy dissipation of the BI CFRP/PBO laminate.

Fig. 9 qualitatively shows the role of Ti foils on the response of BI hybrid interleaved laminate concept impacted at 210 m/s. We notice that the presence of Ti foils precluded the crushing (and severe) fragmentation of the top CFRP block at the impact face due to their higher failure strain compared to CFRP. Nonetheless, as we removed some of the PBO fibres at the back face and replaced them with impact-faced Ti foils (to keep the hybridising ratio constant), the BI Ti/CFRP/PBO laminate concept perforated at 210 m/s (Fig. 9 (b)), which does not repeat the good performance that we observed in the BI CFRP/PBO that withstood the impact and only penetrated, Fig. 9 (a). The difference in response is due to: changing the type and the position of the hybridising material (here Ti foils vs PBO fibres, and impact vs back face), a small change (~0.3 mm) in the total thickness of the laminate, and the number of PBO plies and their pitch angles in each block.

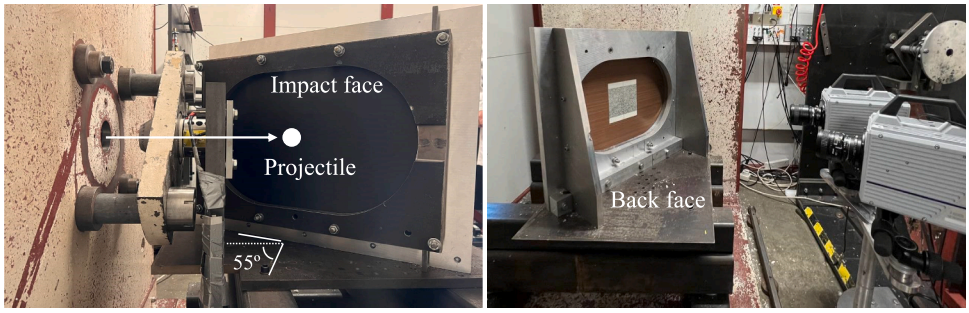
## 3. Demonstrator panels

### 3.1. Design and manufacturing

Since the BI CFRP/PBO laminate concept proved to be the best-




(a) Schematics




(b) Front view (c) Rear view

**Fig. 11.** Test setup for the demonstrator panels.

performing concept among others under HVI, we scaled it up to develop industrial demonstrator panels with a higher target areal weight of 1.5 g/cm$^2$ (chosen for its industrial relevance, compared to 0.95 g/cm$^2$ for the large-scale laminate concepts). To reach the target areal weight of 1.5 g/cm$^2$, we followed the same design methodology and implemented two more blocks of BI CFRP and PBO with a modified number of plies and pitch angles (from 30° to 20° for CFRPs and 7° to 6° for PBOs) to have full rotation(s) in each of the materials, see Fig. 10. In addition, monolithic QI CFRP demonstrator panels with the layup of $(60/0/-60)_{6S}$ are manufactured to compare the results. We used the same manufacturing technique described earlier for the large-scale laminate concepts and manufactured 6 demonstrator panels. In terms of dimensions, we increased the size to 550 × 360 mm for the demonstrator panels (from 225 × 225 mm for the large-scale laminate concepts). The target areal weight of 1.5 g/cm$^2$ increased the average thickness of the large-scale laminate concepts by about 40%.

### 3.2. Testing

To test the demonstrator panels, we used a different test rig [41], see Fig. 11. We used larger and heavier spherical projectiles (approximately three times larger compared to the projectiles used in the previous section) impacting the demonstrator panels at an industrially-relevant incidence angle of 55° (with respect to the normal of the panels, Fig. 11 (b)) to more closely represent a fan blade-off event hitting the engine containment casing. We impacted the panels at an angle to better represent a fan blade-off event onto the containment casing of an aircraft engine. To carry out the tests, we rested each panel against a steel stopper bar and clamped each panel between two profiled fixture plates, see (yellow components in) Fig. 11 (a), which were then bolted onto

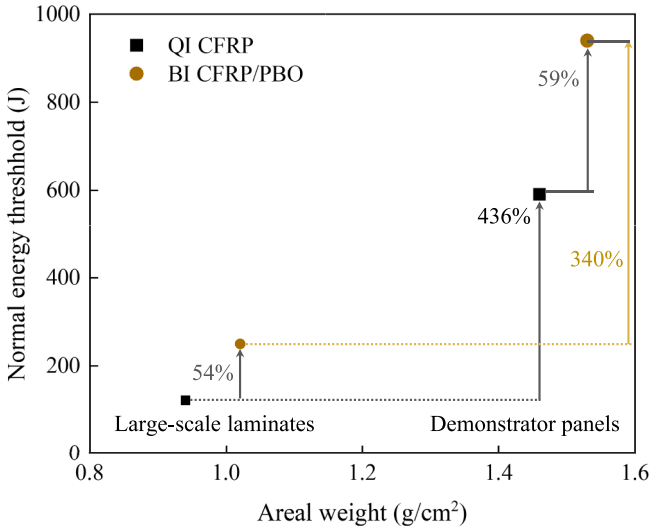



**Fig. 12.** The comparison of normal energy thresholds between large-scale laminates and demonstrator panels.

supports. During bolting, we used a feeler gauge to ensure a clearance of 0.1 mm between the panels and the profiled fixtures to have a reasonable tightness of the mounted panels and avoid potential clamping damage to the panels. We recorded the impact events at a frame rate of 10,000 fps using a Phantom camera mounted above the test setup. To qualitatively monitor the deformation of the panels using 3D digital

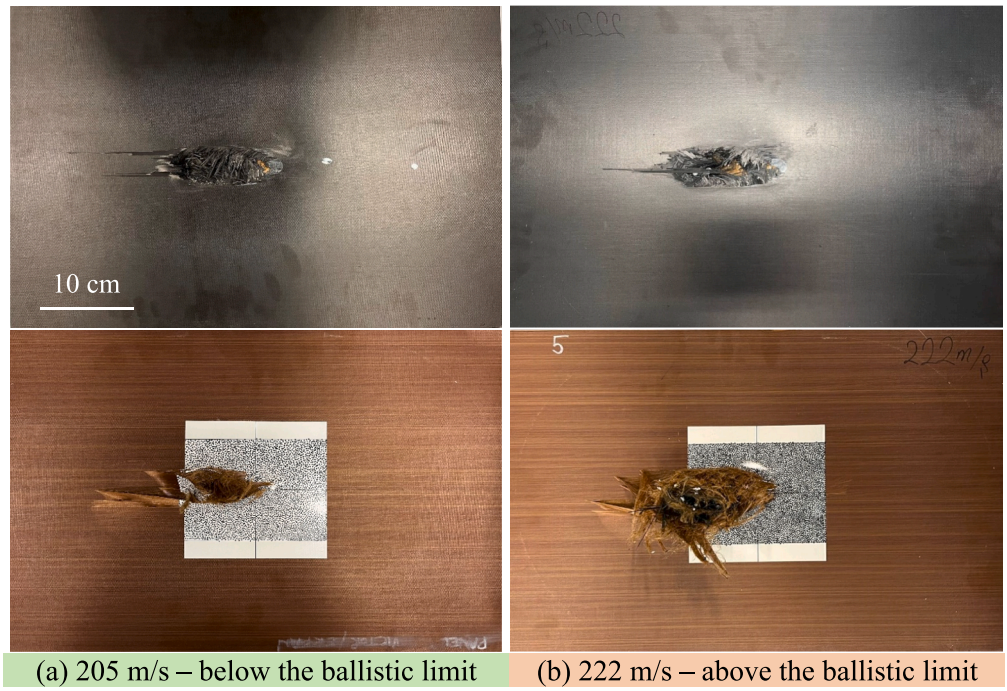



**Fig. 13.** Impact and back faces of the (BI CFRP/PBO) demonstrator panels impacted at 205 and 222 m/s.

image correlation, we painted the back surface of the panels (Fig. 11 (c)) and specked it based on the approach developed in a previous study [41]. We used two Photron cameras (FASTCAM SA5, Photron Ltd, Japan) to record the back surface deformation at a rate of 40,000 fps.

### 3.3. Results and discussion

Fig. 12 compares the normal values of energy threshold between large-scale laminates and demonstrator panels. By scaling up and therefore increasing the areal weight from 0.95 to 1.5 g/cm$^2$, we observe a 436% improvement in the normal energy threshold of the QI CFRP demonstrator panels (baseline). However, for the BI CFRP/PBO demonstrator panels, we observe a smaller improvement, about 340%, in the response. Nonetheless, our bio-inspired hybrid interleaved design methodology still improved the normal energy threshold of the baseline QI design by 59%, which is quite similar to the improvement we observed in the large-scale laminates (54 %), Fig. 12.

Fig. 13 shows the impact face and back face of selected demonstrator panels tested below the ballistic limit at 205 m/s and above the ballistic limit at 222 m/s. By using the Lambert-Jonas equation [39] and fitting the experimental data similar to the large-scale laminate concepts, we obtained a ballistic limit of about 215–220 m/s for the demonstrator panels. Fig. 13 (a) and (b) show that the impact and back faces show significantly localised damage, and neither the impact nor the back face shows extended damage towards the edges of the panels, in contrast to what we previously observed for the large-scale laminates. Moreover, in contrast to the large-scale laminate concepts, the back face of the demonstrator panels, impacted below the ballistic limit, suffered from significant damage and PBO fibre failure, Fig. 13 (a). As a result, the small-scale designs for HVI-resistant CFRP-based laminates cannot be simply assumed to exhibit an equivalent performance for industrial applications with thicker laminates, heavier projectiles and impacts at an angle.

To analyse the internal damage of the panels, we carried out C-scan and cross-sectional analyses of the panels impacted below and above the ballistic limit. As the panels are particularly thick, we carried out the C-scan from both the impact and back face of the panels, Fig. 14. C-scan images of the impact face of the panels show that the panel impacted at

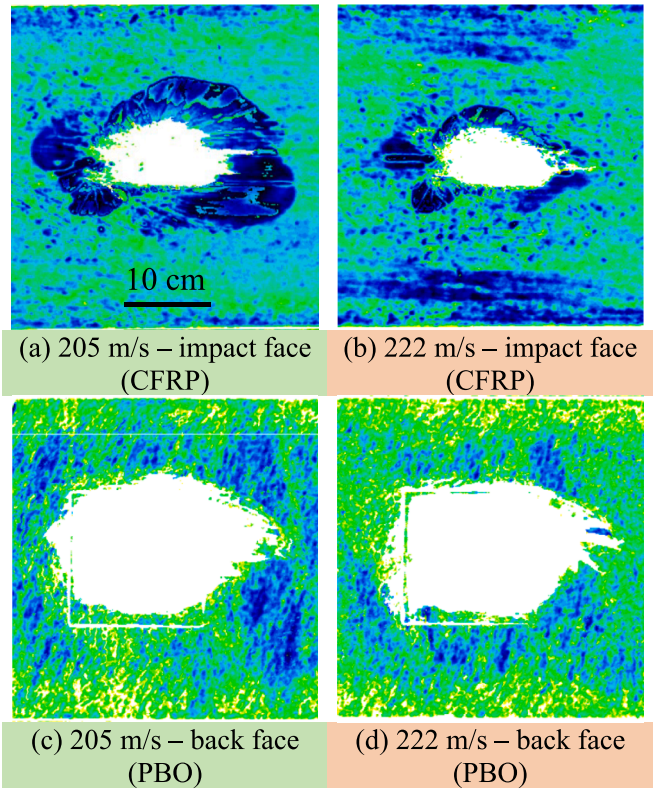



**Fig. 14.** C-scan images of the impact face (CFRP) and back face (PBO) of the demonstrator panels impacted at 205 and 222 m/s.

205 m/s (below the ballistic limit Fig. 14 (a)) underwent more delamination and damage extent compared to the panel impacted at 222 m/s, Fig. 14 (b). This is because, above the ballistic limit, the damage becomes more localised. However, the C-scan images of the panels at both velocities show quite similar responses from the back (PBO) side, but the

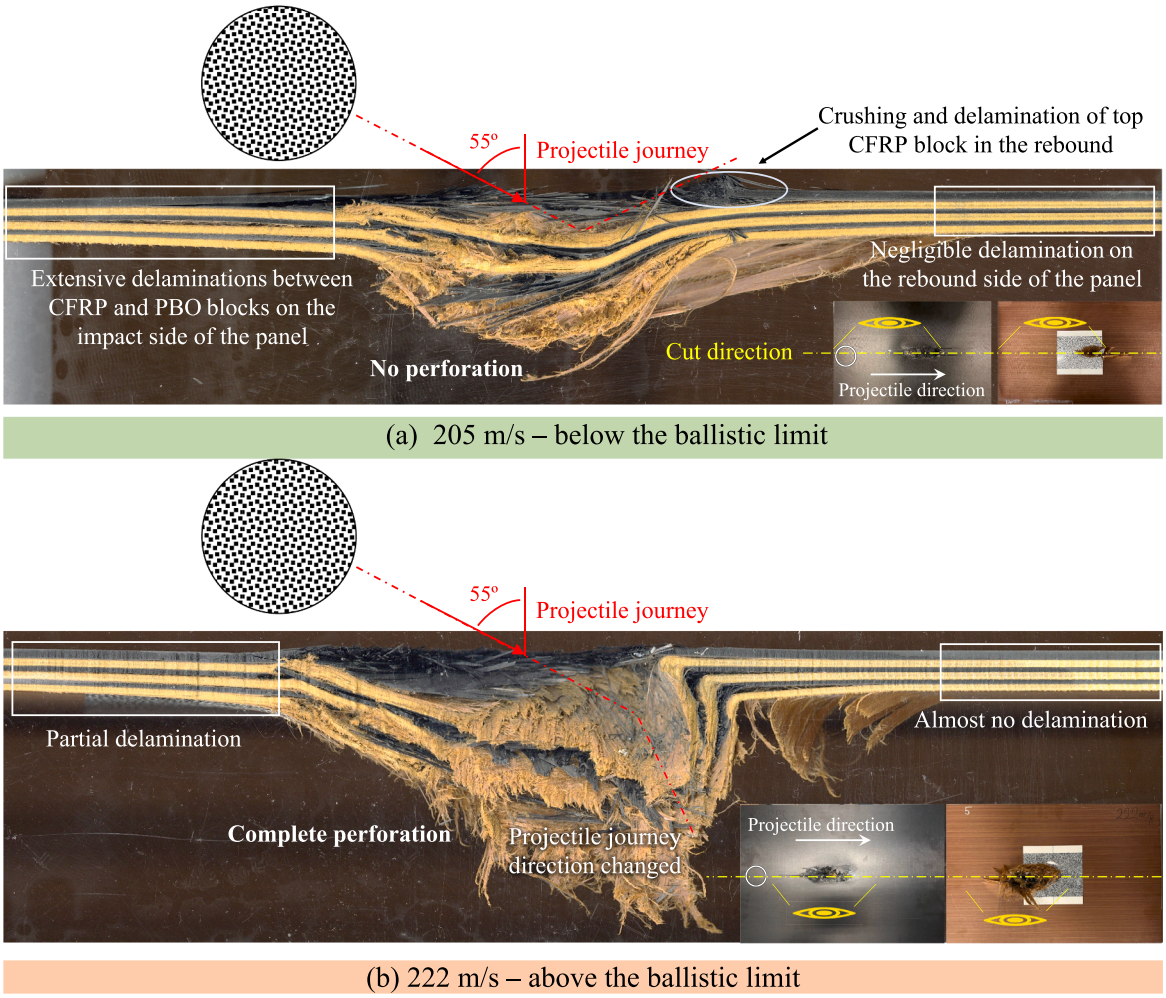



**Fig. 15.** Cross-sections of the demonstrator (BI CFRP/PBO) panels impacted at 205 and 222 m/s.

extent of the damage/delamination is higher since the PBO fibres have higher failure strain compared to CFRPs, Fig. 14 (c) and (d).

Finally, we cut the demonstrator panels impacted at 205 m/s and 222 m/s along their lengths in half and provided their cross-section images in Fig. 15 (a) and (b), respectively, along their corresponding paths of the projectile journeys. As Fig. 15 (a) shows, when the projectile hit the panel at 55°, it rebounded and we observed crushing and delamination of the top CFRP block at the rebound location. Due to the angled impact (and thus normal and tangential components of velocities), we observed extensive delaminations between the blocks of CFRP and PBO at the (left part of the) impact side, in contrast to the (right part of the) rebound side when we observed negligible delamination. Although the projectile did not perforate nor penetrate the panel, we detected severe fibre failure in the blocks of CFRP and the back face block of PBO, due to tensile waves caused by compressive forces, which is in contrast to what we observed in the previous large-scale laminate concepts, where we did not have fibre failure at the back face below the ballistic limit. This behaviour is related to the changes in the specimens and test setup. Nonetheless, we do not observe (significant) damage in the middle blocks of PBO.

By increasing the impact velocity beyond the ballistic limit, we observe perforation in the panels with the projectile exiting the panel at a different angle compared to its impact angle, Fig. 15 (b). The projectile journey shows that, when the projectile hit the panel, the PBO fibres deflected/rotated more than 90°, which guided the projectile and changed its exit path. The CFRPs, on the contrary, due to their brittle response, broke during the impact and did not play a significant role in energy dissipation nor in changing the path of the projectile, compared to PBO fibres. At impact velocities above the ballistic limit, we did not detect (significant) delamination in the areas away from the impact zone, Fig. 15 (b), which contrasts with what we observed previously in the large-scale laminate concepts.

## 4. Conclusions

In this study, we applied a novel design methodology consisting of bio-inspired (BI) helicoidal and interleaved designs to develop hybrid carbon fibre-reinforced polymer (CFRP) composite laminates suitable for aerospace applications subject to high-velocity impact (HVI).

Firstly, we developed and manufactured large-scale CFRP-based laminate concepts including: BI monolithic CFRP, BI hybrid interleaved CFRP/PBO, and BI hybrid interleaved Ti/CFRP/PBO with the dimensions of 225 × 225 mm and the target areal weight of 0.95 g/cm$^2$. We then tested the developed laminate concepts under HVI ranging from 150 to 300 m/s. We calculated the ballistic limits and investigated the response in terms of energy dissipation and failure modes and compared them with that of the equivalent monolithic quasi-isotropic (QI) CFRP counterpart. We found that:

- replacing the QI layup of the monolithic CFRP baseline with the BI layup resulted in an increase of about 29% in ballistic limit and about 15% in specific energy dissipation;
- the large-scale CFRP/PBO laminate concept performed best among other developed concepts with 21% higher energy dissipation

compared to the Ti/CFRP/PBO laminate, with 34% higher energy dissipation compared to the monolithic BI laminate, and with 54% higher energy dissipation compared to the traditional monolithic QI baseline; and

- the large-scale CFRP/PBO laminate concept also showed the highest ballistic limit among various developed laminates with a ballistic limit of about 212 m/s; following this, Ti/CFRP/PBO showed the second highest ballistic limit of 197 m/s; monolithic BI had a slightly lower ballistic limit of about 190 m/s, and the traditional monolithic QI baseline showed the lowest ballistic of 147 m/s.

Taking into account that the large-scale CFRP/PBO laminate concept proved to be the best-performing design, we scaled it up for an industrial demonstrator and manufactured panels with dimensions of 550 × 360 mm and a target areal weight of 1.50 g/cm$^2$. We tested them under HVI at an industrially-relevant angle of 55° with a larger and heavier projectile to more closely represent a fan blade-off event hitting the casing. We found that the changes in the test setup configurations, namely scaling the laminate up, testing at an angle and using a larger and heavier projectile, significantly affected the failure mechanisms and ballistic limit.

This study shows that small-scale designs for HVI-resistant CFRP-based laminates cannot be simply assumed to exhibit an equivalent performance for industrial applications with thicker laminates, heavier projectiles and impacts at an angle. We suggest that, for developing industrial-scale composite structures subject to ballistic impacts, full-sized laminates along with real test conditions should be used to obtain reliable designs.

## CRediT authorship contribution statement

**M. Erfan Kazemi:** Conceptualization, Formal analysis, Investigation, Methodology, Visualization, Writing – original draft, Writing – review & editing. **Victor Medeau:** Conceptualization, Formal analysis, Investigation, Methodology. **Yanhong Chen:** Investigation, Writing – original draft. **Ziwen Xu:** Investigation, Writing – original draft. **Nik Petrinic:** Resources, Supervision, Funding acquisition. **Emile Greenhalgh:** Funding acquisition, Resources, Supervision. **Paul Robinson:** Funding acquisition, Resources, Supervision. **James Finlayson:** Conceptualization, Project administration, Resources. **Silvestre T. Pinho:** Conceptualization, Funding acquisition, Methodology, Project administration, Supervision, Writing – review & editing.

## Declaration of competing interest

The authors declare that they have no known competing financial interests or personal relationships that could have appeared to influence the work reported in this paper.

## Data availability

The data that has been used is confidential.

## Acknowledgements

The funding from Innovate UK under the UKRI FANDANGO project No. 113232 (https://gtr.ukri.org/projects?ref=113232) is gratefully acknowledged.

## Appendix A. Supplementary material

Supplementary data to this article can be found online at https://doi.org/10.1016/j.compositesa.2023.107992.

## References

[1] El-Sayed AF. Bird strike in aviation: statistics, analysis and management. John Wiley & Sons; 2019.
[2] Thorpe J. Fatalities and destroyed civil aircraft due to bird strikes, 1912-2002. In: International Bird Strike Committee, 26th Meeting Warsaw, Poland; 2003. p. 28.
[3] Ćwiklak J, Kobiałka E, Goś A. Experimental and numerical investigations of bird models for bird strike analysis. Energies 2022;15(10):3699.
[4] Salehi H, Ziaei-Rad S, Vaziri-Zanjani M. Bird impact effects on different types of aircraft bubble windows using numerical and experimental methods. Int J Crashworthiness 2010;15(1):93–106.
[5] Shupikov A, Ugrimov S, Smetankina N, Yareshchenko V, Onhirsky G, Ukolov V, et al. Bird dummy for investigating the bird-strike resistance of aircraft components. J Aircr 2013;50(3):817–26.
[6] Yang B. Blade containment evaluation of civil aircraft engines. Chin J Aeronaut 2013;26(1):9–16.
[7] Cosme N, Chevrolet D, Bonini J, Peseux B, Cartraud P. Prediction of engine loads and damages due to fan blade off event. In: 43rd AIAA/ASME/ASCE/AHS/ASC Structures, Structural Dynamics, and Materials Conference; 2002. p. 1666.
[8] Cosme N, Chevrolet D, Bonini J, Peseux B, Cartraud P. Prediction of transient engine loads and damage due to hollow fan blade-off. Revue Européenne des Eléments 2002;11(5):651–66.
[9] Liu S, Chen W, Chen M. Failure Assessment of Aero-engine Support Structure due to Blade-off. Trans Nanjing Univ Aeronaut Astronaut 2018;35(5):838–48.
[10] Kassapoglou C. Design and analysis of composite structures: with applications to aerospace structures. John Wiley & Sons; 2013.
[11] Irving P, Soutis C. Polymer composites in the aerospace industry. Woodhead Publishing; 2019.
[12] Mrazova M. Advanced composite materials of the future in aerospace industry. Incas Bull 2013;5(3):139.
[13] Wagner T, Heimbs S, Franke F, Burger U, Middendorf P. Experimental and numerical assessment of aerospace grade composites based on high-velocity impact experiments. Compos Struct 2018;204:142–52.
[14] Davies GAO, Olsson R. Impact on composite structures. Aeronaut J 2004;108 (1089):541–63.
[15] Reyes Villanueva G, Cantwell WJ. The high velocity impact response of composite and FML-reinforced sandwich structures. Compos Sci Technol 2004;64(1):35–54.
[16] Kazemi ME, Shanmugam L, Lu D, Wang X, Wang B, Yang J. Mechanical properties and failure modes of hybrid fiber reinforced polymer composites with a novel liquid thermoplastic resin, Elium®. Compos A Appl Sci Manuf 2019;125:105523.
[17] Cantwell W, Morton J. Impact perforation of carbon fibre reinforced plastic. Compos Sci Technol 1990;38(2):119–41.
[18] Hazell P, Appleby-Thomas GJ, Kister G. Impact, penetration, and perforation of a bonded carbon-fibre-reinforced plastic composite panel by a high-velocity steel sphere: an experimental study. J Strain Anal Eng Des 2010;45(6):439–50.
[19] Heimbs S, Wagner T, Viana Lozoya JT, Hoenisch B, Franke F. Comparison of impact behaviour of glass, carbon and Dyneema composites. Proc Inst Mech Eng C J Mech Eng Sci 2019;233(3):951–66.
[20] Tirillò J, Ferrante L, Sarasini F, Lampani L, Barbero E, Sánchez-Sáez S, et al. High velocity impact behaviour of hybrid basalt-carbon/epoxy composites. Compos Struct 2017;168:305–12.
[21] Li X, Zhang X, Guo Y, Shim V, Yang J, Chai GB. Influence of fiber type on the impact response of titanium-based fiber-metal laminates. Int J Impact Eng 2018; 114:32–42.
[22] Zulkifli F, Stolk J, Heisserer U, Yong A-T-M, Li Z, Hu XM. Strategic positioning of carbon fiber layers in an UHMwPE ballistic hybrid composite panel. Int J Impact Eng 2019;129:119–27.
[23] Li X, Zhang X, Zhang H, Yang J, Nia AB, Chai GB. Mechanical behaviors of Ti/CFRP/Ti laminates with different surface treatments of titanium sheets. Compos Struct 2017;163:21–31.
[24] Sun J, Xu S, Lu G, Wang Q, Gong A. Ballistic impact experiments of titanium-based carbon-fibre/epoxy laminates. Thin-Walled Struct 2022;179:109709.
[25] Kazemi ME, Shanmugam L, Dadashi A, Shakouri M, Lu D, Du Z, et al. Investigating the roles of fiber, resin, and stacking sequence on the low-velocity impact response of novel hybrid thermoplastic composites. Compos B Eng 2021;207:108554.
[26] Nisini E, Santulli C, Ceruti A, Liverani A. High speed impact properties of carbon-basalt-flax DHEC composites compared with pure carbon fibre composites. Compos Struct 2018;192:165–72.
[27] da Silva AAX, Scazzosi R, Manes A, Amico SC. High-velocity impact behavior of aramid/S2-glass interply hybrid laminates. Appl Compos Mater 2021;28(6): 1899–917.
[28] Kazemi ME, Medeau V, Greenhalgh E, Robinson P, Finlayson J, Pinho ST. Bio-inspired interleaved hybrids: Novel solutions for improving the high-velocity impact response of carbon fibre-reinforced polymers (CFRP). Composites Part B: Engineering 2023;264:110930.
[29] Bouligand Y. Twisted fibrous arrangements in biological materials and cholesteric mesophases. Tissue Cell 1972;4(2):189–217.
[30] Mencattelli L, Pinho ST. Realising bio-inspired impact damage-tolerant thin-ply CFRP Bouligand structures via promoting diffused sub-critical helicoidal damage. Compos Sci Technol 2019;182:107684.
[31] Ginzburg D, Pinto F, Iervolino O, Meo M. Damage tolerance of bio-inspired helicoidal composites under low velocity impact. Compos Struct 2017;161: 187–203.
[32] Jiang H, Ren Y, Liu Z, Zhang S, Lin Z. Low-velocity impact resistance behaviors of bio-inspired helicoidal composite laminates with non-linear rotation angle based layups. Compos Struct 2019;214:463–75.

[33] Yang F, Xie W, Meng S. Global sensitivity analysis of low-velocity impact response of bio-inspired helicoidal laminates. Int J Mech Sci 2020;187:106110.
[34] Wang C, Su D, Xie Z, Wang H, Hazell PJ, Zhang Z, et al. Dynamic behaviour of Bio-inspired heterocyclic aramid Fibre-reinforced laminates subjected to Low-velocity Drop-weight impact. Compos A Appl Sci Manuf 2022;153:106733.
[35] Liu JL, Mencattelli L, Zhi J, Chua PY, Tay T-E, Tan VBC. Lightweight, Fiber-Damage-Resistant, and Healable Bio-Inspired Glass-Fiber Reinforced Polymer Laminate. Polymers 2022;14(3):475.
[36] Wang H, Wang C, Hazell PJ, Wright A, Zhang Z, Lan X, et al. Insights into the high-velocity impact behaviour of bio-inspired composite laminates with helicoidal lay-ups. Polym Test 2021;103:107348.
[37] Abir MR, Tay TE, Lee HP. On the improved ballistic performance of bio-inspired composites. Compos A Appl Sci Manuf 2019;123:59–70.
[38] Kazemi ME MV, Mencattelli L, Greenhalgh E, Robinson P, Finlayson J, Pinho S. Bio-inspired interleaved hybrids: novel solutions for improving the high-velocity impact response of carbon fibre-reinforced polymers (CFRP). Compos Part B: Eng. 2023; Manuscript submitted for publication.
[39] Lambert J, Jonas G. Towards standardization in terminal ballistics testing: velocity representation. Army ballistic research lab aberdeen proving ground MD; 1976.
[40] Alonso L, Martínez-Hergueta F, Garcia-Gonzalez D, Navarro C, García-Castillo S, Teixeira-Dias F. A finite element approach to model high-velocity impact on thin woven GFRP plates. Int J Impact Eng 2020;142:103593.
[41] Quino G, Chen Y, Ramakrishnan KR, Martínez-Hergueta F, Zumpano G, Pellegrino A, et al. Speckle patterns for DIC in challenging scenarios: rapid application and impact endurance. Meas Sci Technol 2020;32(1):015203.